

Electronic Supplementary Information

Thickness Control of 3-Dimensional Mesoporous Silica Ultrathin Films by Wet-Etching

Maho Kobayashi,^{a,†} Kyoka Susuki,^{a,†} Tomohiro Otani,^b Shinpei Enomoto,^c Haruo Otsuji,^c Yoshiyuki Kuroda,^d Hiroaki Wada,^a Atsushi Shimojima,^a Takayuki Homma,^{a, b} and Kazuyuki Kuroda^{*, a, c}

^aDepartment of Applied Chemistry, Faculty of Science and Engineering, Waseda University, 3-4-1 Ohkubo, Shinjuku-ku, Tokyo 169-8555, Japan. E-mail: kuroda@waseda.jp

^bDepartment of Advanced Science and Engineering, Faculty of Science and Engineering, Waseda University, 3-4-1 Ohkubo, Shinjuku-ku, Tokyo 169-8555, Japan.

^c Kagami Memorial Research Institute for Materials Science and Technology, Waseda University, 2-8-26 Nishiwaseda, Shinjuku-ku, Tokyo 169-0051, Japan.

^d Waseda Institute for Advanced Study, 1-6-1 Nishiwaseda, Shinjuku-ku, Tokyo 169-8050, Japan.

[†]These authors equally contributed to this paper.

Table of Contents

1. Preparation of mesoporous silica thin films thinner than conventional ones by a bottom-up process.

Figure S1 Mesoporous silica thin films prepared from precursor solutions with higher ratios of ethanol over precursor solutions (our results).

2. Experimental Details.

2.1 Preparation of 3-dimensional mesoporous silica thin films (3MPSF_as).

2.2 Electrodeposition of CoPt into the mesoporous silica ultrathin films.

Table S1 Bath composition.

Table S2 Electrodeposition conditions.

2.3 Details on the SEM observations of both surface and cross-section of 3MPSF_as and 3MPSF_et

Figure S2 Preparation of specimens for SEM observations of both the surface and cross-section of 3MPSF_as and 3MPSF_et.

3. Characterization details of 3-dimensional mesoporous silica thin films (3MPSF_as).

3.1 Optical microscopy.

Figure S3 Typical optical microscopy image of the surface of 3MPSF_as.

3.2 X-ray diffraction.

Figure S4 Models of *Fmmm* structure.

Figure S5 $\theta-2\theta$ XRD patterns of 3MPSF_as and 3MPSF_et using the drop casting method (aq. NH_4F , 0.1 M).

3.3 SEM observations.

4. Fabrication of mesoporous silica ultrathin films using the drop casting method.

Figure S6 2D-XRD patterns of 3MPSF_et2h and 4h using the drop casting method (aq. NH_4F , 0.1 M).

Figure S7 SEM images of the surfaces of 3MPSF_et1h, 2h and 4h using the drop casting method (aq. NH_4F , 0.1 M).

Figure S8 SEM images of 3MPSF_as and 3MPSF_et using the drop casting method (aq. NH_4F , 0.1 M).

Figure S9 Observations of 3MPSF_et2h using the drop casting method (aq. NH_4F , 0.1 M).

Figure S10 XPS spectra of the surface of 3MPSF_as and 3MPSF_et4h using the drop casting method (aq. NH_4F , 0.1 M).

5. Application of the drop casting method using different etching conditions.

5.1 Variations in the etching solutions.

Figure S11 Characterization of 3MPSF_et4h using the drop casting method (aq. NH_4F , (a) 0.01 M and (b) 0.05 M).

Figure S12 Characterization of 3MPSF_et using the drop casting method (aq. NaOH , 0.01 M, (a) 30 min and (b) 1 h).

Figure S13 Characterization of 3MPSF_et using the drop casting method (aq. HF , 0.01 M, (a) 10 min and (b) 30 min).

5.2 Variation in the film thickness.

Figure S14 SEM image of Cross-section of thicker 3MPSF_as.

Figure S15 2D-XRD patterns of thicker 3MPSF_as and 3MPSF_et using the drop casting method (aq. NH_4F , 0.1 M).

5.3 Variation in the lateral size of the film.

Figure S16 2D-XRD patterns and SEM images of 3MPSF_as and 3MPSF_et2h with size of 2 cm by 2 cm using the drop casting method (aq. NH_4F , 0.1 M).

6. Wet-etching of 3MPSF_as by immersion in an aq. NH_4F .

Figure S17 2D-XRD patterns of 3MPSF_as and 3MPSF_et using the immersion method (aq. NH_4F , 0.1 M).

Figure S18 SEM images of the surface of 3MPSF_et3h using the immersion method (aq. NH_4F , 0.1 M).

7. Etching process of the drop casting method.

Figure S19 Photographs of 3- μL water on 3MPSF_as and 3MPSF_et using the drop casting method (aq. NH_4F , 0.1 M) for contact angle measurements (0h: 50°, 1h: 20°, 2–4h: 0°).

8. Preparation of nanodot patterns within mesoporous silica ultrathin films.

Figure S20 2D-XRD patterns of 3MPSF_as_Ru-sub and 3MPSF_et_Ru-sub using the drop casting method (aq. NH_4F , 0.1 M).

Figure S21 SEM images of the surfaces and cross-sections of 3MPSF_as_Ru-sub and 3MPSF_et_Ru-sub using the drop casting method (aq. NH_4F , 0.1 M).

Figure S22 Current profiles during potentiostatic electrodeposition of CoPt (a) into 3MPSF_et_Ru-sub and (b) on bare Ru substrate.

Figure S23 XPS spectra of CoPt nanodot patterns before and after removal of silica.

REFERENCES

1. Preparation of mesoporous silica thin films thinner than conventional ones by a bottom-up process.

Although a very thin mesoporous silica film is able to be prepared as the amount of solvent (ex: ethanol) becomes larger, the ordering becomes lower, and 3D and 2D phases are often mixed, as shown in Figure S1. Hussen et al. reported the same findings.¹ Our results as well as those reported previously suggest that thinner 3D mesoporous silica thin films are difficult to be prepared by the EISA method in general. Our result also shows that the reproducibility is low.

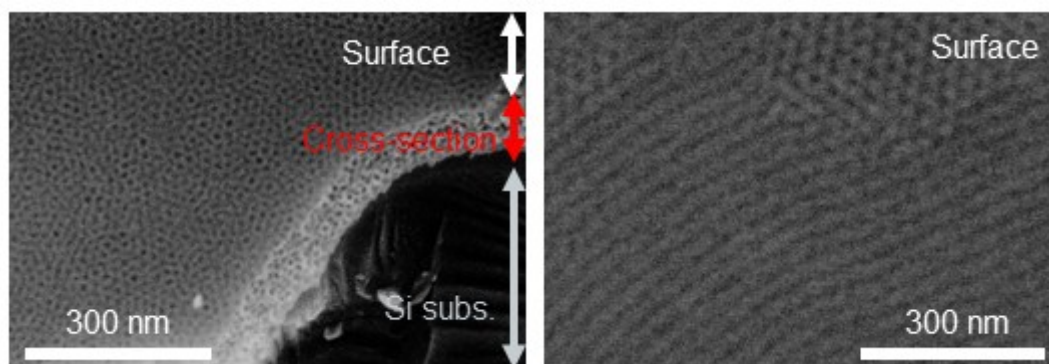


Figure S1

SEM images of mesoporous silica thin films prepared from precursor solutions with higher ratios of ethanol over precursor solutions (our results). Disordered 3D mesoporous silica thin film (left) and mesoporous silica thin film with mixed 3D and 2D mesostructures (right).

2. Experimental Details.

2.1 Preparation of 3-dimensional mesoporous silica thin films (3MPSF_as).

A mesoporous silica thin film was prepared on a Si (100) substrate by the EISA method according to a previous report.² Tetraethoxysilane (TEOS), ethanol (EtOH), deionized water (H₂O), and HCl were mixed for 30 min at 60 °C, and a surfactant solution (Pluronic F127 as the template and EtOH) was added and the mixture was stirred for another 30 min at room temperature. Finally the molar ratio was TEOS : F127 : H₂O : HCl : EtOH = 1 : 0.0029 : 9.2 : 0.021 : 51. This precursor solution was dip-coated on a Si substrate (2 × 2 cm) at a withdrawal rate of 0.5 mm/sec, at 25 °C, and 65% RH, and a mesostructured silica thin film was formed. The films were dried at 70 °C for 8 h in air and then calcined in air at a heating rate of 1 °C/min, and kept at 440 °C for 4 h to give as-made mesoporous silica thin films (3MPSF_as).

2.2 Electrodeposition of CoPt into the mesoporous silica ultrathin films.

The following conditions were employed for the deposition.

Table S1 Bath composition.

		Reagents	Conc./mM
Complexing agent	Diammonium hydrogen citrate	(NH ₄) ₂ C ₄ H ₆ O ₇	100
Complexing agent	Glycine	NH ₂ CH ₂ COOH	100
Co source	Cobalt(II) sulfate heptahydrate	CoSO ₄ · 7H ₂ O	100
Pt source	Diamminedinitroplatinum(II)	Pt(NO ₂) ₂ (NH ₃) ₂	2.1

Table S2 Electrodeposition conditions.

Bath temperature	30 °C
Working electrode	3MPSF_et_Ru-sub
Reference electrode	Ag/AgCl
Counter electrode	Co wire
Applied potential	−900 mV
Deposition time	8 min
pH	5.2

2.3 Details on the SEM observations of both surface and cross-section of 3MPSF_as and 3MPSF_et.

The films were scratched with a diamond pen along the dot-line in Figure S2 (left) for SEM observations of both the surface and cross-section of the films (Figure S2 (right)).

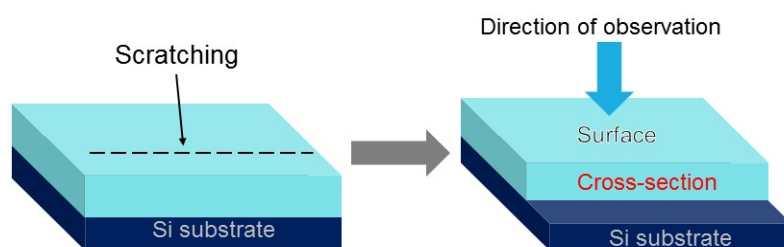
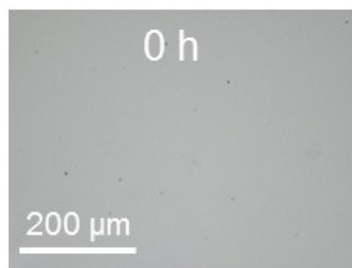


Figure S2 Preparation of specimens for SEM observations of both the surface and cross-section of 3MPSF_as and 3MPSF_et. Please note that the cross-sections of the film are not fabricated at a completely right angle by scratching the film with a diamond pen.

3. Characterization details of 3-dimensional mesoporous silica thin films (3MPSF_as).

3.1 Optical microscopy.

A typical optical microscopic image of 3MPSF_as (Figure S3) shows a continuous smooth surface. Other optical images are not shown because they are basically same. Interference color was not observed, which suggests that the film was



very thin.

Figure S3 Typical optical microscopy image of the surface of 3MPSF_as.

3.2 X-ray diffraction.

The relative positions of spots in the 2D-XRD pattern of 3MPSF_as (Figure 3) are same as those of a previous report,³ showing the mesostructure with *Fm $\bar{3}$ m* symmetry. Three intense spots are assignable to 020, 111, and 002 diffractions of the structure, as indicated in the figure. These assignments, taking the *b*-axis perpendicular to the substrate (the (020) plane parallel to the substrate), are based on the model shown in Figure S4. The θ -2 θ XRD profile of 3MPSF_as (Figure S5) shows one peak arising from the perpendicular periodicity corresponding to d_{020} . The unit cell parameters with the *Fm $\bar{3}$ m* symmetry were calculated using the d values of both 2D-XRD (Figure 3) and θ -2 θ XRD (Figure S5). Because the ultrathin films have very small numbers of repeated planes, the d values are not precisely determined. The following parameters are roughly estimated. The b parameter was calculated to be 13.5 nm on the basis of d_{020} (6.77 nm). The c parameter was calculated to be 26 nm by using the value of d_{002} of the 2D-XRD pattern (13 nm). The a parameter was 18 nm by using the value of c (26 nm / $\sqrt{2}$) and the relationship of $a : c$ is 1 : $\sqrt{2}$ (Figure S4),³ when the film structure takes *Fm $\bar{3}$ m* with the b axis perpendicularly oriented to the substrate. All the spots including those under the extinction rule of *Fm $\bar{3}$ m* symmetry were simulated by Crystal Maker, using the calculated unit cell parameters, and all the positions are superimposed on the observed 2D-XRD pattern (Figure 3). All the spots observed in the 2D-XRD pattern are perfectly fitted with spots calculated from the simulation.

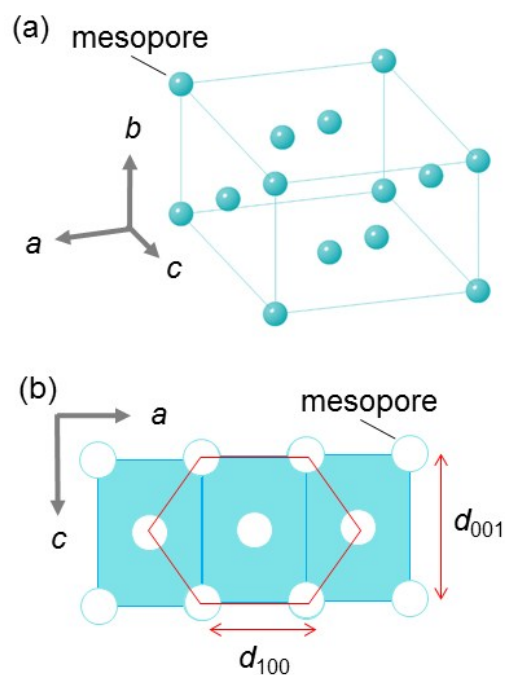


Figure S4 Models of *Fmmm* structure.

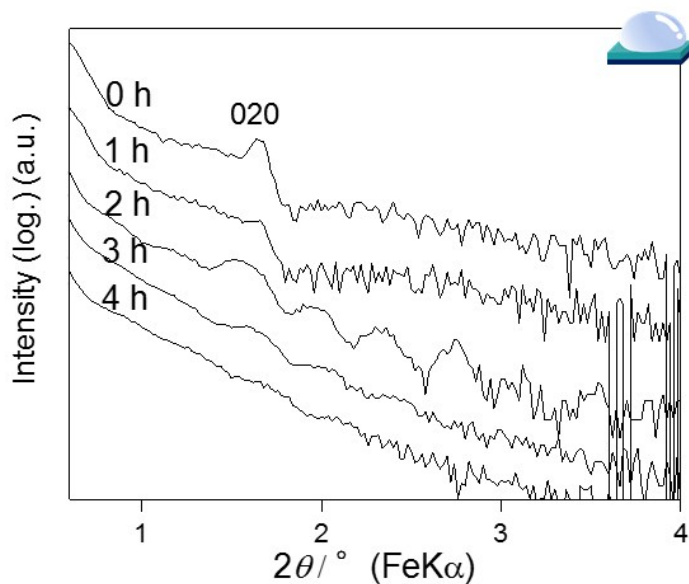


Figure S5 θ - 2θ XRD patterns of 3MPSF_as and 3MPSF_et using the drop casting method (aq. NH_4F , 0.1 M).

3.3 SEM observations.

The SEM images of the surface of 3MPSF_as under the accelerating voltage of

3 kV (Figure 4) show that the dark spots correspond to mesopores and that the distance between mesopores was ca. 18 nm and ca. 27 nm, which is almost in accordance with values of d_{100} and d_{001} of the *Fmmm* structure, respectively (please see Figure S4(b)). The FFT pattern of the SEM image (Figure 4(0 h), inset) shows that mesopores are arranged in an elongated hexagonal manner in the *a-c* plane and the ratio of the size is $1 : \sqrt{2}$ (please see Figure S4(b)). The arrangement corresponds to the (010) plane of *Fmmm* symmetry. This result also supports that the film mesostructure takes the *Fmmm* symmetry.

As described above, all the characterization results of 3MPSF_{as} support the formation of 3-dimensional orthorhombic (*Fmmm*) mesoporous silica thin films with cell parameters of $a = 18$ nm, $b = 13.5$ nm and $c = 26$ nm and with the *b*-axis oriented perpendicularly to the substrate.

4. Fabrication of mesoporous silica ultrathin films using the drop casting method.

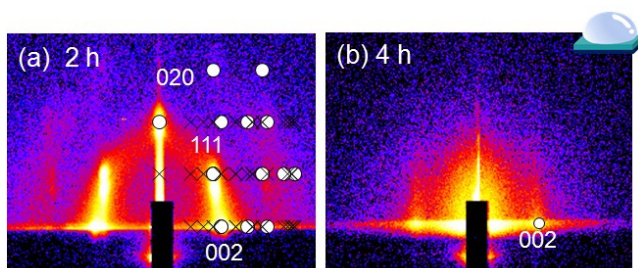


Figure S6 2D-XRD patterns of 3MPSF_et2h and 4h using the drop casting method (aq. NH_4F , 0.1 M). The specimens were prepared separately from the samples described in the main text, which supports the reproducibility of the method. Open circles represent diffraction peaks calculated from *Fmmm* symmetry and crosses represent positions calculated from the extinction rule.

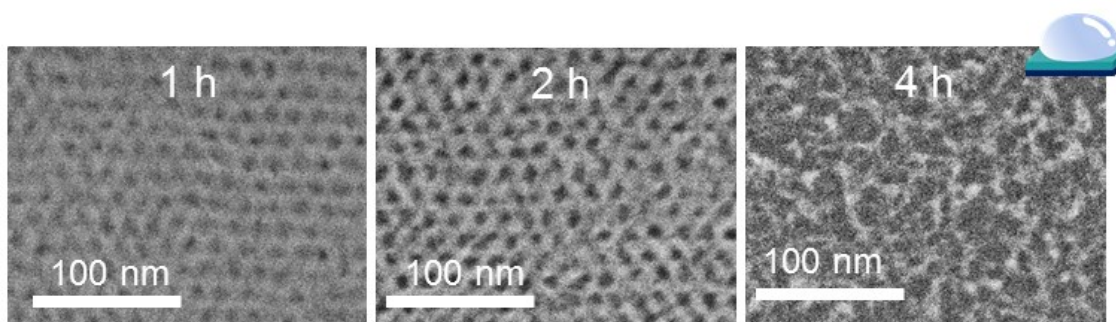


Figure S7 SEM images of the surfaces of 3MPSF_et1h, 2h, and 4h using the drop casting method (aq. NH_4F , 0.1 M). The specimens were prepared separately from the samples described in the main text.

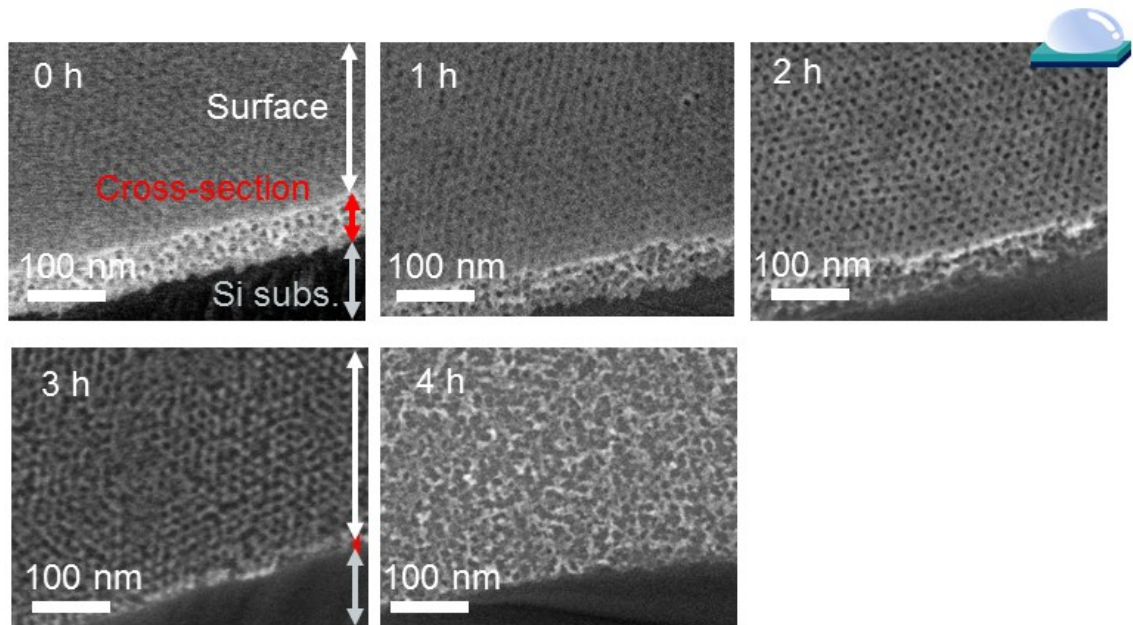


Figure S8 SEM images of 3MPSF_{as} and 3MPSF_{et} using the drop casting method (aq. NH₄F, 0.1 M). The specimens of 0 h and 3 h were prepared separately from those of 1 h, 2 h, and 4 h.

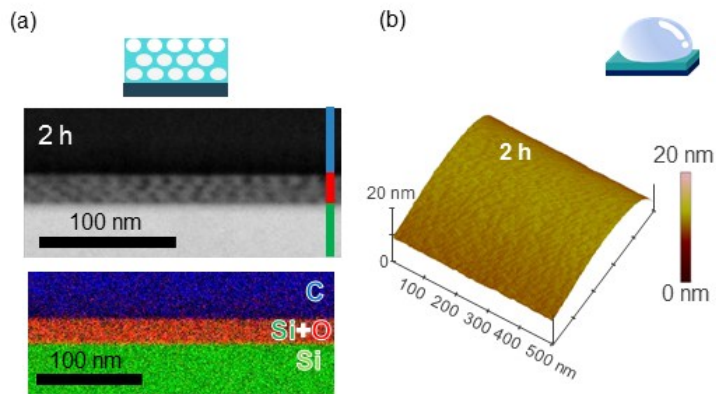


Figure S9 Observations of 3MPSF_{et2h} using the drop casting method (aq. NH₄F, 0.1 M). (a) Cross-sectional HAADF-STEM image (upper) and EDS mapping image (lower) and (b) AFM image of the surface. The specimen was prepared separately from the sample presented in the main text.

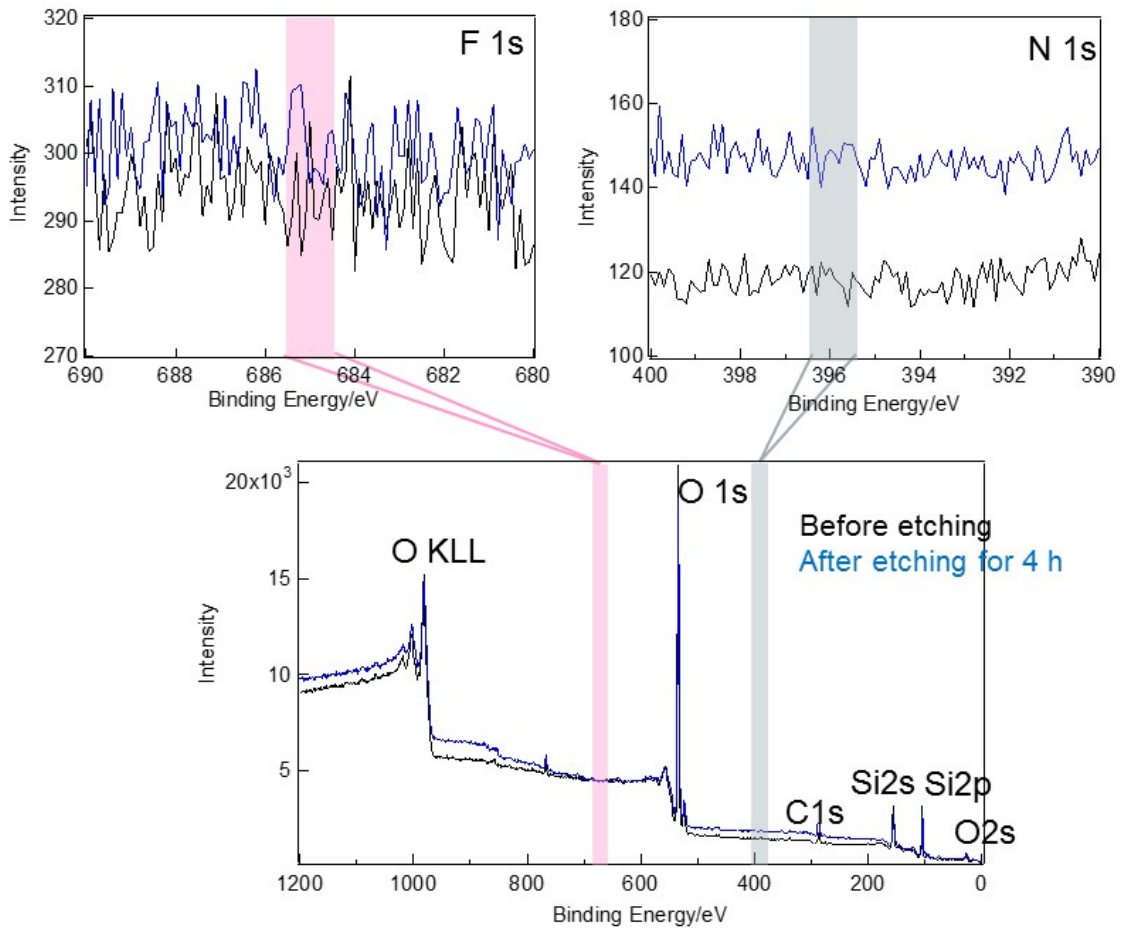


Figure S10 XPS spectra of the surface of 3MPSF_as and 3MPSF_et4h prepared by using the drop casting method (aq. NH_4F , 0.1 M).

5. Application of the drop casting method using different etching conditions.

5.1 Variations in the etching solutions.

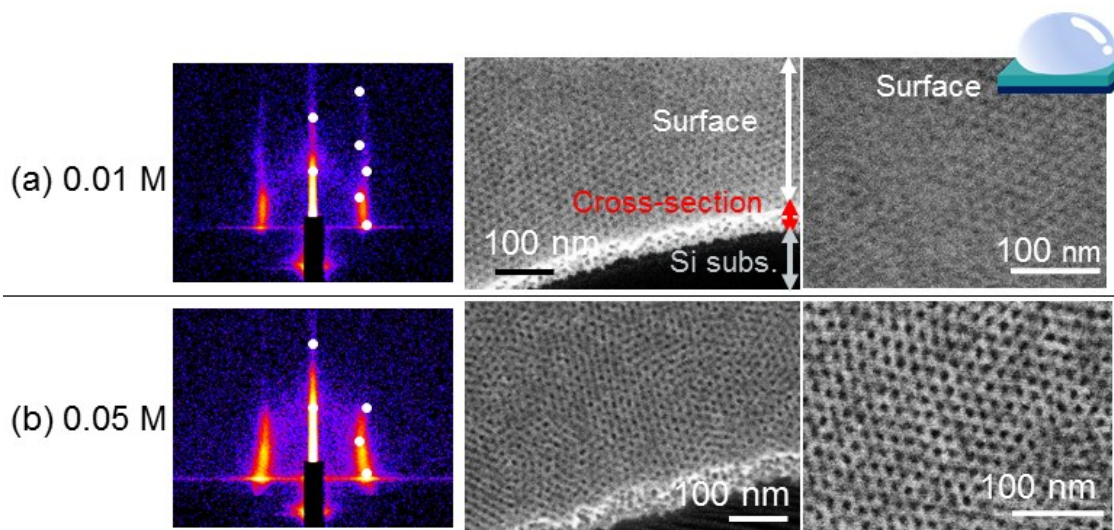


Figure S11 Characterization of 3MPSF_et4h using the drop casting method (aq. NH₄F, (a) 0.01 M and (b) 0.05 M). (Left) 2D-XRD patterns. (Center and right) SEM images. The 2D-XRD pattern of 3MPSF_et4h using 0.01 M shows higher order diffraction spots, which indicates that the film thickness is thicker and/or that the vertical periodicity is higher than those found for the case for 3MPSF_et4h using 0.05 M (where the 2D-XRD pattern did not show higher order spots.). Therefore, the use of aq. NH₄F (0.01 M) results in the slower etching rate. The 2D-XRD pattern with higher contrast is not directly related to the ordering. Furthermore, the SEM images of both of the samples clearly show the slower etching rate for the case of 0.01M because the surface of the film treated with 0.01 M has a surface silica layer while the sample treated with 0.05 M shows that the surface silica layers were removed or became very thin.

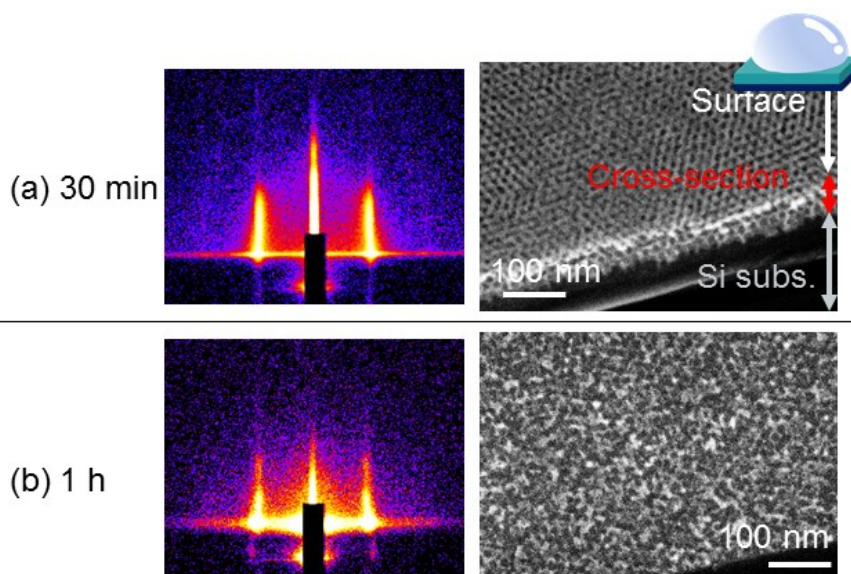


Figure S12 Characterization of 3MPSF_et using the drop casting method (aq. NaOH, 0.01 M, (a) 30 min and (b) 1 h). (Left) 2D-XRD patterns. (Right) SEM images.

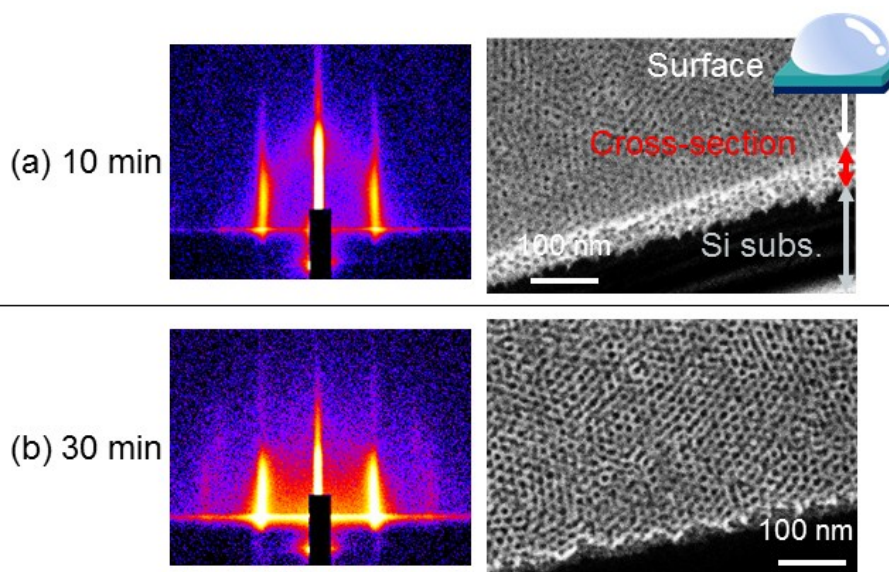


Figure S13 Characterization of 3MPSF_et using the drop casting method (aq. HF, 0.01 M, (a) 10 min and (b) 30 min). (Left): 2D-XRD patterns. (Right) SEM images.

5.2 Variation in the film thickness.

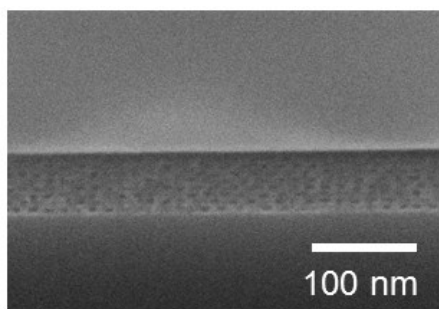


Figure S14 SEM image of cross-section of thicker 3MPSF_{as}.

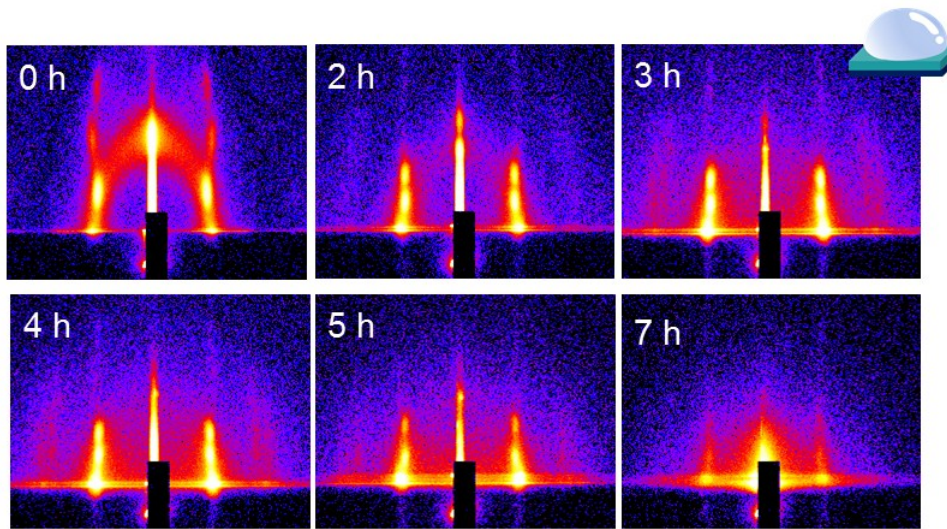


Figure S15 2D-XRD patterns of thicker 3MPSF_{as} and 3MPSF_{et} using the drop casting method (aq. NH₄F, 0.1 M).

5.3 Variation in the lateral size of the film.

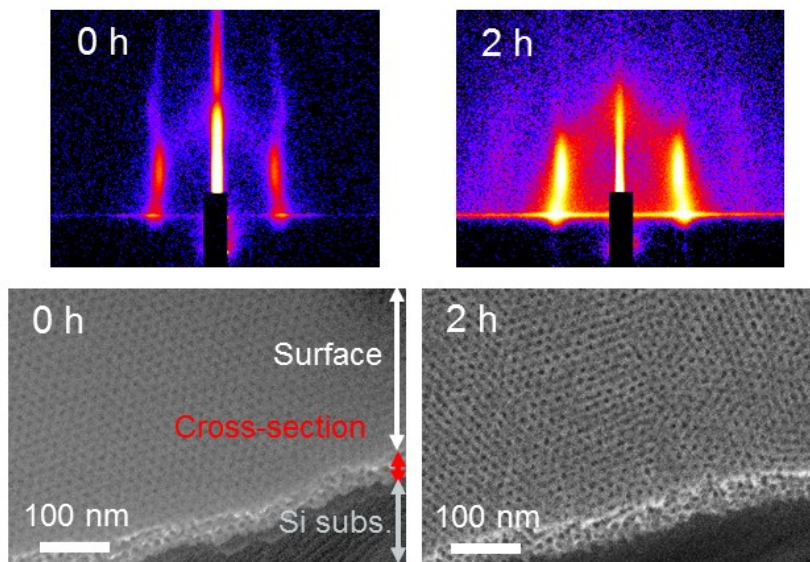


Figure S16 2D-XRD patterns and SEM images of 3MPSF_{as} and 3MPSF_{et2h} with the size of 2 cm by 2 cm using the drop casting method (aq. NH₄F, 0.1 M).

6. Wet-etching of 3MPSF_as by immersion in an aq. NH_4F .

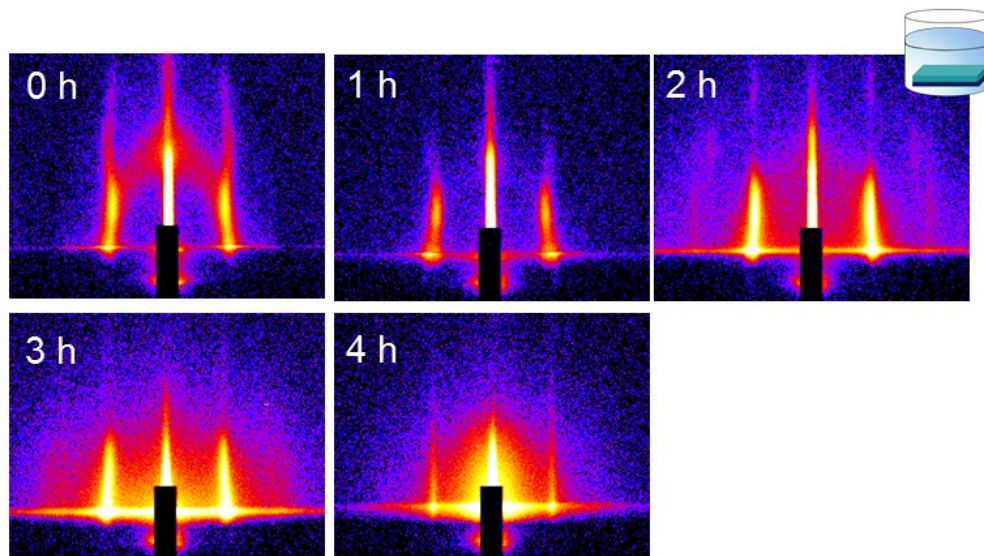


Figure S17 2D-XRD patterns of 3MPSF_as and 3MPSF_et prepared by using the immersion method (aq. NH_4F , 0.1 M).

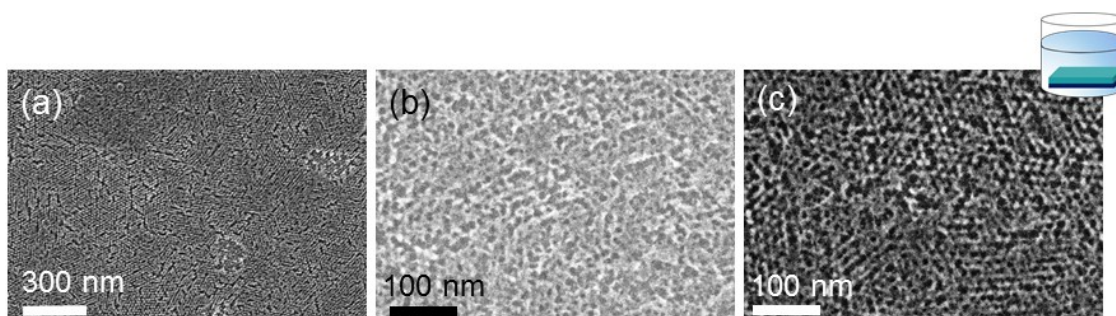


Figure S18 SEM images of the surface of 3MPSF_et3h prepared by using the immersion method (aq. NH_4F , 0.1 M). (a) Image taken with lower magnification. (b) Image taken at the center of specimen. (c) Image taken at the edge of specimen.

7. Etching process of the drop casting method.

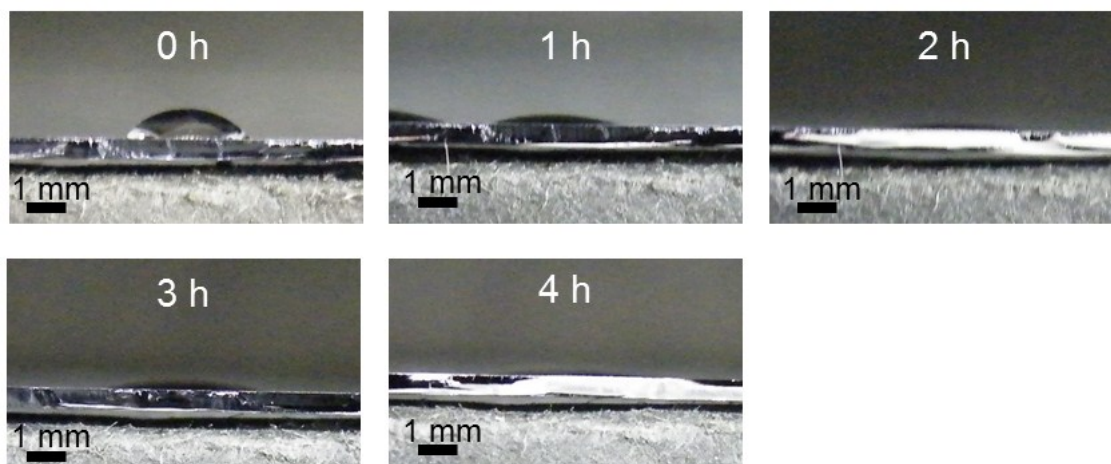


Figure S19 Photographs of 3- μ L water on 3MPSF_{as} and 3MPSF_{et} prepared by using the drop casting method (aq. NH_4F , 0.1 M) for contact angle measurements (0h: ca. 50°, 1h: ca. 20°, 2–4h: ca. 0°).

8. Preparation of nanodot patterns within mesoporous silica ultrathin films.

The 2D-XRD pattern of 3MPSF_as_Ru-sub (Figure S20(0 h)) was same as that of 3MPSF_as on a Si-sub, indicating that the film has the same mesostructure (*Fmmm*). After etching, the spots assignable to the vertical periodicity disappeared and the spots assignable to the in-plane periodicity were observed with decrease in the relative intensity of the spot (Figure S20(2 h)), indicating that the mesostructure was retained.

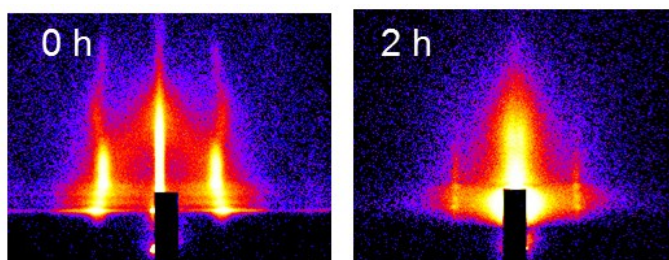


Figure S20 2D-XRD patterns of 3MPSF_as_Ru-sub and 3MPSF_et_Ru-sub using the drop casting method (aq. NH_4F , 0.1 M).

The SEM images of the films before and after etching for 2 h are shown in Figure S21. The surface SEM images show a highly-ordered arrangement of mesopores for the film before etching and lower ordering of mesostructure for the film after etching. The cross-sectional SEM images show that the film thickness was about 30 nm for the film before etching, and about 15 nm for the film after etching. These results are consistent with those of 2D-XRD data.

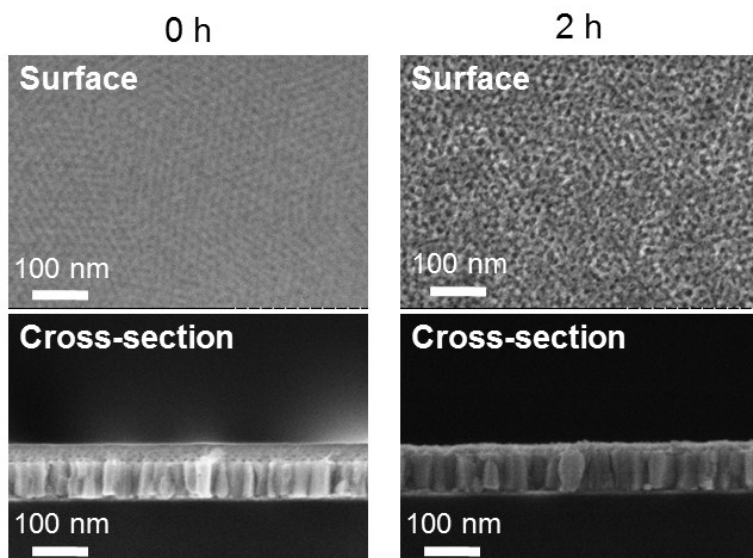


Figure S21 SEM images of the surfaces and cross-sections of 3MPSF_as_Ru-sub and 3MPSF_et_Ru-sub prepared by using the drop casting method (aq. NH_4F , 0.1 M).

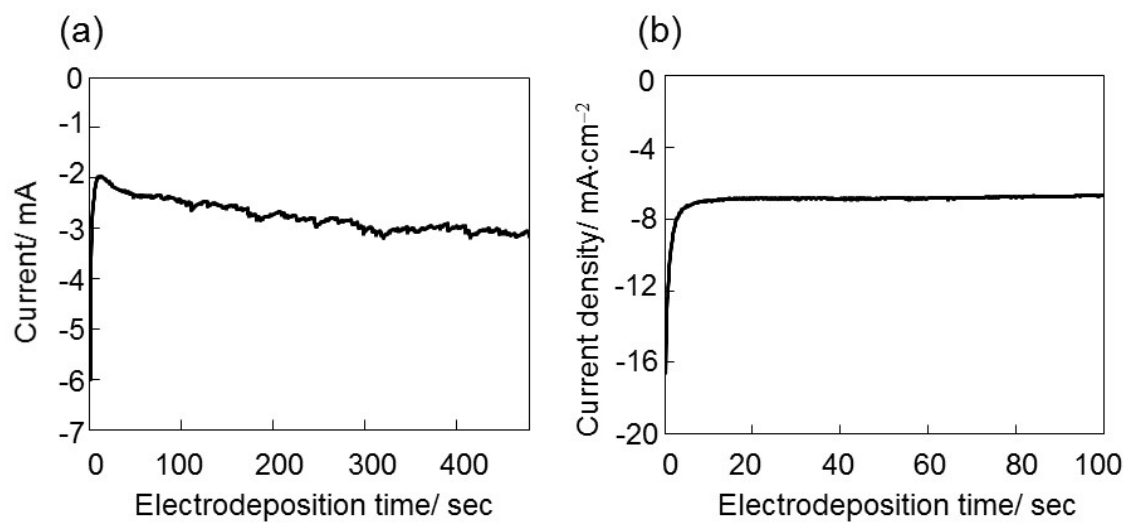


Figure S22 Current profiles during potentiostatic electrodeposition of CoPt (a) into 3MPSF_et_Ru-sub and (b) on bare Ru substrate.

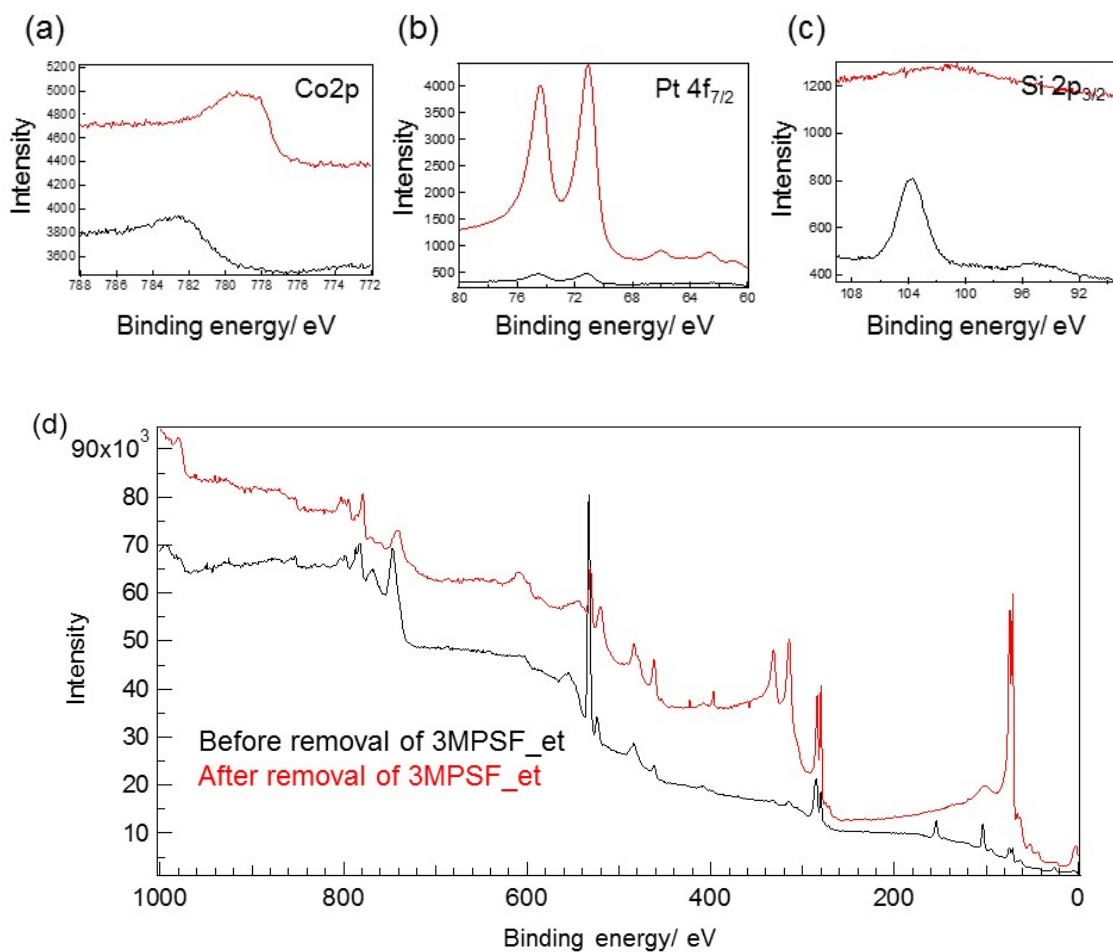


Figure S23 XPS spectra of CoPt nanodot patterns before and after removal of silica. (a) Co 2p. (b) Pt 4f_{7/2}. (c) Si 2p_{3/2}. (d) wide region.

Before removal of silica, the peak assigned to Co 2p was observed at 782.6 eV, suggesting the formation of Co(OH)₂ owing to the deposition conditions. After the removal of silica with conc. aq. NaOH, metallic Co was exposed, resulting in the observation of metallic Co peak (780.0 eV) in the spectra.

REFERENCES

- 1 G. N. A. Hussen, H. Shirakawa, W. D. Nix and B. M. Clemens, *J. Appl. Phys.*, 2006, **100**, 114322-1.
- 2 H. Daiguji, J. Hwang, A. Takahashi, S. Kataoka and A. Endo, *Langmuir*, 2012, **28**, 3671.
- 3 P. Falcaro, D. Grosso, H. Amenitsch and P. Innocenzi, *J. Phys. Chem. B*, 2004, **108**, 10942.